

COMPLEMENTARITY OF STACKING AND MULTIPLIET CONSTRAINTS ON THE BLAZAR CONTRIBUTION TO THE CUMULATIVE HIGH-ENERGY NEUTRINO INTENSITY

CHENGCHAO YUAN¹, KOHTA MURASE^{1,2}, AND PETER MÉSZÁROS¹*Draft version May 28, 2022*

ABSTRACT

We investigate the blazar contribution to the cumulative neutrino intensity assuming a generic relationship between neutrino and gamma-ray luminosities, $\log(L_\nu) \propto \log(L_{\text{ph}})$. Using the gamma-ray luminosity functions for blazars including flat spectrum radio quasars (FSRQs) and BL Lac objects, as well as the *Fermi*-LAT detection efficiency, we estimate contributions from resolved blazars and all blazars. Combining the existing upper limits from stacking analyses, the cumulative neutrino flux from all blazars are constrained. We also evaluate effects of the redshift evolution and the effective local number densities for each class of FSRQs, BL Lacs, and all blazars, by which we place another type of constraints on the blazar contribution using the non-detection of high-energy neutrino multiplets. We demonstrate that these two upper limits are complementary, and the joint consideration of stacking and multiplet analyses support arguments that blazars are disfavored as the dominant sources in the 100 TeV neutrino sky.

Subject headings: galaxies: active – neutrinos

1. INTRODUCTION

Since the initial detection of high-energy astrophysical neutrinos by the IceCube Neutrino Observatory (Aartsen et al. 2013a,b), a cumulative flux of astrophysical neutrinos in the energy range from ~ 10 TeV to several PeV has been unveiled and measured to a higher precision (Aartsen et al. 2014a, 2015a, 2016). The isotropic distribution of the cumulative flux as well as the background-only results from recent searches for point-like sources and multi-messenger analyses support an extragalactic origin of these neutrinos (Ahlers & Murase 2014; Aartsen et al. 2014b, 2015b). Up to now, however, the main origin of the cumulative neutrinos still remains unknown.

The flavor ratio measured at Earth, $(\nu_e : \nu_\mu : \nu_\tau) \approx (1 : 1 : 1)$, is consistent with the prediction from the long-distance oscillations of neutrinos produced through pion decays (Aartsen et al. 2015c), which provides one common framework for the astrophysical models dedicated to explain the cumulative neutrino flux. Many candidates have been proposed and studied (see Ahlers & Halzen 2015; Mészáros 2017, for review). Among these candidates, blazars, which are known as a subclass of AGNs with a relativistic jet pointing nearly towards the Earth, have been frequently considered as the ultra-high-energy cosmic-ray (CR) accelerators and high-energy neutrino emitters (Murase 2017). Recently, the IceCube collaboration announced the spatial and temporal coincidence between a muon track neutrino event IceCube170922A and a blazar TXS 0506+056 (IceCube Collaboration et al. 2018) at the significance $3 - 4\sigma$. Intuitively, if this association is physical, the intimate link between this IceCube neutrino event and the blazar could favor blazars as the main sources of the cumulative neu-

trino flux, but this is not the case (Murase et al. 2018).

The maximum likelihood stacking searches for cumulative neutrino flux from second *Fermi*-LAT AGN catalog (2LAC) as well as the point-source searches using the IceCube muon track events and blazars in *Fermi* 3LAC have independently shown that blazars only contribute a small portion of the IceCube cumulative neutrino flux (Aartsen et al. 2017a; Pinat & Sánchez 2017; Hooper et al. 2018) and the hadronic models of blazar activity are strongly constrained (Neronov et al. 2017). Palladino et al. (2019) evaluated the contribution of unresolved sources, and showed that the blazar contribution to the cumulative neutrino flux is constrained unless one makes an ad hoc assumption that lower-luminosity blazars entrain a larger amount of cosmic rays (CRs). Also, the non-detection of neutrinos from nearby blazars such as Mrk 421 also give interesting constraints (Aartsen et al. 2014b; Ando et al. 2017; IceCube Collaboration et al. 2019) and may disfavor blazars as the dominant origin of IceCube neutrinos.

The absence of clustering in high-energy neutrino events, i.e., neutrino multiplets and auto-correlation, also provides constraints on various classes of proposed sources as the dominant origin of the cumulative neutrino flux (Murase & Waxman 2016; Ahlers & Halzen 2014; Aartsen et al. 2014b; Feyereisen et al. 2017; Glauch et al. 2017; Dekker & Ando 2019). The constraints are sensitive to the redshift evolution of the sources, which are especially powerful for weakly or non-evolving sources such as BL Lac objects (Murase & Waxman 2016; Murase et al. 2018). But the limits are weaker for rapidly evolving sources such as FSRQs, which could significantly alleviate the constraints as remarked by Murase et al. (2018). Neronov & Semikoz (2018) studied the constraints on evolving blazar populations and confirmed that fast evolving sources (e.g. $\xi_z = 5.0$) may indeed relax the multiplet limits.

In this work, we consider “joint” implications of these independent analyses. We introduce a generic relation-

cxy52@psu.edu

¹ Department of Physics; Department of Astronomy & Astrophysics; Center for Particle and Gravitational Astrophysics, The Pennsylvania State University, University Park, PA 16802, USA² Center for Gravitational Physics, Yukawa Institute for Theoretical Physics, Kyoto University, Kyoto, Kyoto 606-8502, Japan

ship between neutrino and gamma-ray luminosities, as $L_\nu \propto L_{\text{ph}}^{\gamma_{\text{lw}}}$. Physically, the correlation between L_ν and L_{ph} is determined by the interactions between particles and radiation fields inside the sources. Most of physically reasonable models developed on the basis of photo-hadronic (e.g. $p\gamma$) interactions predict $L_\nu \propto L_{\text{ph}}^{\gamma_{\text{lw}}}$ with indices of $1.0 \lesssim \gamma_{\text{lw}} \lesssim 2.0$ (e.g., Murase et al. 2014; Dermer et al. 2014; Tavecchio & Ghisellini 2015; Petropoulou et al. 2015; Padovani et al. 2015; Murase & Waxman 2016; Righi et al. 2017; Murase et al. 2018; Rodrigues et al. 2018). The index γ_{lw} characterizes the source models and may deviate from this fiducial range for models with increasing complexity. Motivated by that, treating γ_{lw} as a free parameter, we reveal the γ_{lw} -dependence of the upper limits on blazar contributions.

In the first part (§2), we calculate the ratio of neutrino fluxes from resolved blazars and all blazars. Combining this ratio with the existing constraints on resolved blazars, we estimate the upper limits for all-blazar contributions. The multiplet constraints are given in the second part (§3) where we also derive the effective number densities $n_0^{\text{eff}}(\gamma_{\text{lw}})$ and the redshift evolution factor $\xi_z(\gamma_{\text{lw}})$ for blazars and the subclasses, FSRQs and BL Lacs. In either case, we use the blazar gamma-ray luminosity functions provided by Ajello et al. (2015, 2012, 2013) to reconstruct the neutrino luminosity density. In §4 we conclude with a discussion.

2. IMPLICATIONS OF STACKING LIMITS

Given the differential density of blazars as a function of rest-frame 100MeV-100GeV luminosity L_{ph} , redshift z and photon index Γ defined by the gamma-ray flux $F \propto \varepsilon_{\text{ph}}^{-\Gamma}$,

$$\frac{d^3 N_{\text{bl}}}{dL_{\text{ph}} dz d\Gamma} = \phi_{\text{bl}}(L_{\text{ph}}, z) \frac{dP_{\text{bl}}}{d\Gamma} \frac{dV}{dz}, \quad (1)$$

where the subscript “bl” represents blazars considered in the calculation, $\phi_{\text{bl}}(L_{\text{ph}}, \Gamma) = d^2 N_{\text{bl}}/dL_{\text{ph}} d\Gamma$ is the luminosity function and $dP_{\text{bl}}/d\Gamma$ is the probability distribution of spectral index Γ , we can directly write down the luminosity density of neutrinos from resolved blazars at redshift z ,

$$\begin{aligned} \varepsilon_\nu Q_\nu^{(\text{bl}, \text{R})}(z, \gamma_{\text{lw}}) &= \int_{L_{\text{ph}, \text{th}}}^{L_{\text{ph}, \text{max}}} \int_{\Gamma_{\text{min}}}^{\Gamma_{\text{max}}} \phi_{\text{bl}}(L_{\text{ph}}, z) L_\nu(L_{\text{ph}}) \\ &\times \frac{dP_{\text{bl}}}{d\Gamma} d\Gamma dL_{\text{ph}} \end{aligned} \quad (2)$$

where $L_\nu \propto L_{\text{ph}}^{\gamma_{\text{lw}}}$ is the neutrino luminosity, $L_{\text{ph}, \text{max}}$ is a fixed upper limit of blazar luminosity and the lower limit $L_{\text{ph}, \text{th}}(L_{\text{ph}}, z, \Gamma)$ is determined by the *Fermi* LAT threshold flux $F_{100, \text{th}}$ in the energy range 100 MeV \sim 100 GeV. For a blazar at redshift z with the luminosity $L_{\text{ph}} \propto \int_{\varepsilon_{\text{min}}}^{\varepsilon_{\text{max}}} F(\varepsilon) \varepsilon d\varepsilon$, where $\varepsilon_{\text{max}} = 100(1+z)$ GeV and $\varepsilon_{\text{min}} = 100(1+z)$ MeV, and the photon index Γ , the

integrated flux at earth can be written as

$$F_{100}(L_{\text{ph}}, z, \Gamma) = \frac{L_{\text{ph}}}{4\pi d_L^2(z)} \times \begin{cases} \ln\left(\frac{\varepsilon_{\text{max}}}{\varepsilon_{\text{min}}}\right) \frac{1}{\varepsilon_{\text{max}} - \varepsilon_{\text{min}}} & \Gamma = 1 \\ \frac{\varepsilon_{\text{max}} \varepsilon_{\text{min}} \ln\left(\frac{\varepsilon_{\text{max}}}{\varepsilon_{\text{min}}}\right)}{\varepsilon_{\text{max}} - \varepsilon_{\text{min}}} & \Gamma = 2 \\ \frac{2-\Gamma}{1-\Gamma} \frac{\varepsilon_{\text{max}}^{1-\Gamma} - \varepsilon_{\text{min}}^{1-\Gamma}}{\varepsilon_{\text{max}} - \varepsilon_{\text{min}}} & \Gamma \neq 1, 2, \end{cases} \quad (3)$$

where d_L is the luminosity distance between the blazar and the detector. Then the lower limit of the integral in equation 2 can be obtained by requiring $F_{100}(L_{\text{ph}, \text{th}}, z, \Gamma) = F_{100, \text{th}}$. Alternatively, thanks to the *Fermi*-LAT detection efficiency $\epsilon(F_{100})$ provided by Abdo et al. (2010), we can simplify the equation 2 by using the equivalent detection efficiency $\epsilon(L_{\text{ph}}, z, \Gamma) = \epsilon(F_{100})$,

$$\begin{aligned} \varepsilon_\nu Q_\nu^{(\text{bl}, \text{R})}(z, \gamma_{\text{lw}}) &= \int_{L_{\text{ph}, \text{min}}}^{L_{\text{ph}, \text{max}}} \int_{\Gamma_{\text{min}}}^{\Gamma_{\text{max}}} \phi_{\text{bl}}(L_{\text{ph}}, z) L_\nu(L_{\text{ph}}) \\ &\times \epsilon(L_{\text{ph}}, z, \Gamma) \frac{dP_{\text{bl}}}{d\Gamma} d\Gamma dL_{\text{ph}}, \end{aligned} \quad (4)$$

where the lower limit $L_{\text{ph}, \text{min}}$ reduces to a constant and represents the minimal luminosity of the sample that contains all blazars. To eliminate the instrumental selection effect produced by the low detection efficiency for dimmer blazars and to take all blazars into account, we replace the $L_{\text{ph}, \text{th}}$ in equation 2 by $L_{\text{ph}, \text{min}}$, which yields the neutrino luminosity density from all blazars $\varepsilon_\nu Q_\nu^{(\text{bl}, \text{all})}(z, \gamma_{\text{lw}})$. Meanwhile, using the LFs and parameters provided by Ajello et al. (2012, 2013), we successfully reproduced the blazar and BL Lac luminosities illustrated in the Figure 6 of Ajello et al. (2013).

Assuming the neutrino spectra from all blazars have the similar power-law form, e.g. $\varepsilon_\nu^2 \Phi_{\varepsilon_\nu} \propto \varepsilon_\nu^{2-s}$, and using the comoving neutrino luminosities $\varepsilon_\nu Q_\nu^{(\text{bl}, \text{all})}(z, \gamma_{\text{lw}})$ and $\varepsilon_\nu Q_\nu^{(\text{bl}, \text{R})}(z, \gamma_{\text{lw}})$, the all-flavor neutrino fluxes from resolved and all blazars at earth are expected to be

$$E_\nu^2 \Phi_{E_\nu}^{(\text{bl}, \text{R}/\text{all})}(\gamma_{\text{lw}}) = \frac{c}{4\pi} \mathcal{C}^{-1} \int dz \varepsilon_\nu^{2-s} \frac{\varepsilon_\nu Q_\nu^{(\text{bl}, \text{R}/\text{all})}(z, \gamma_{\text{lw}})}{(1+z)} \left| \frac{dt}{dz} \right|, \quad (5)$$

where $\varepsilon_\nu = (1+z)E_\nu$ and \mathcal{C} is the normalization coefficient determined by $\varepsilon_{\text{CR}, \text{max}}$ and $\varepsilon_{\text{CR}, \text{min}}$, the maximum and minimum energy that CRs in blazars can achieve. In this work, we assume that the maximum CR energy is the same for all blazars, as is the normalization factor once the spectral index s is specified. Therefore, we can write down the fraction of resolved blazars to the cumulative neutrino flux in a simple way that depends only on γ_{lw} ,

$$\mathcal{F}(\gamma_{\text{lw}}) = \frac{E_\nu^2 \Phi_{E_\nu}^{(\text{bl}, \text{R})}(\gamma_{\text{lw}})}{E_\nu^2 \Phi_{E_\nu}^{(\text{bl}, \text{all})}(\gamma_{\text{lw}})}. \quad (6)$$

Ajello et al. (2015) presented the best-fit parameters in the blazar luminosity functions ϕ_{bl} , which enables us to compute $\mathcal{F}(\gamma_{\text{lw}})$. The redshift correction to the energies introduces one extra term $(1+z)^{2-s}$ to the integrand in equation 5 and another factor $(1+z)^{-1}$ to the integrated flux in equation 3. As a consequence, low-redshift blazars

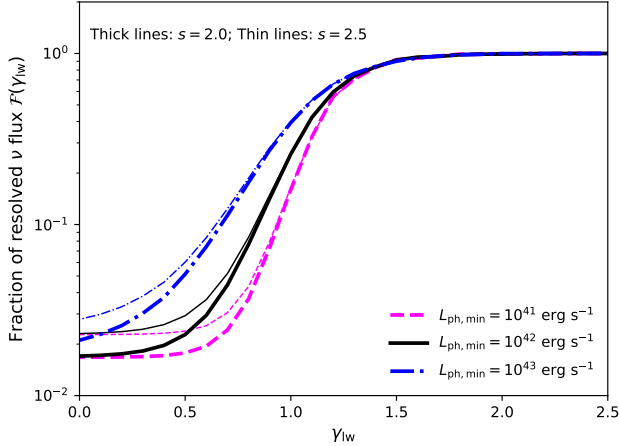


FIG. 1.— The fraction of resolved blazars in the cumulative neutrino flux, $\mathcal{F}(\gamma_{lw})$. The thick and thin lines are calculated for the neutrino spectral indices $s = 2.0$ and $s = 2.5$. The blue dashed, black solid and red dash-dotted lines correspond to the minimum luminosities $L_{ph,min} = 10^{41} \text{ erg s}^{-1}$, $10^{42} \text{ erg s}^{-1}$ and $10^{43} \text{ erg s}^{-1}$, respectively. The upper limit is fixed to be $L_{ph,max} = 10^{50} \text{ erg s}^{-1}$.

become more important when $s = 2.5$ in comparison with the $s = 2$ case. Therefore, considering nearby blazars are easier to be detected, a steeper neutrino spectrum predicts a larger $\mathcal{F}(\gamma_{lw})$, which is confirmed by the thin lines in Figure 1. Note that the selection of the minimum and maximum luminosities, e.g. $L_{ph,min}$ and $L_{ph,max}$ of a blazar is arbitrary. We found that the results are not sensitive to $L_{ph,max}$ while $\mathcal{F}(\gamma_{lw})$ changes dramatically in the range $\gamma_{lw} \lesssim 1.0$ as $L_{ph,min}$ increases from $10^{41} \text{ erg s}^{-1}$ to $10^{43} \text{ erg s}^{-1}$, as shown in Figure 1. Intuitively, a lower $L_{ph,min}$ implies that more low-luminosity blazars in the sample are less likely to be detected. Also, for a weaker luminosity dependance ($\gamma_{lw} \lesssim 1.0$), the low-luminosity blazars dominate the luminosity density due to the large population. The joint affect is that $\mathcal{F}(\gamma_{lw})$ decreases dramatically in the range $\gamma_{lw} \lesssim 1.0$.

Remarkably, from Figure 1, we can conclude that the contribution from resolved blazars is nearly the same as the neutrino flux from all blazars when γ_{lw} is larger than 1.0. The reason is that, assuming a stronger luminosity dependance, the brighter blazars become increasingly important. These high-luminosity blazars have a higher chance to be detected and in this case the neutrinos luminosity densities from resolved blazars and all blazars are comparable. To compute the upper limit of cumulative neutrino flux from all blazars, we use the existing constraints, $E_\nu^2 \Phi_{E_\nu}^{(2LAC, \text{stacking})}$ and $E_\nu^2 \Phi_{E_\nu}^{(3LAC, \text{stacking})}$, from blazar stacking analysis (Aartsen et al. 2017a) and point-source searches (Hooper et al. 2018) based respectively on *Fermi* 2LAC and 3LAC blazars. Combining with the fraction of resolved neutrino flux, we estimate the upper limits of all-blazar contributions from *Fermi* 2LAC and 3LAC analysis,

$$E_\nu^2 \Phi_{E_\nu}^{(2LAC/3LAC)} = \frac{E_\nu^2 \Phi_{E_\nu}^{(2LAC/3LAC, \text{stacking})}}{\mathcal{F}(\gamma_{lw})}. \quad (7)$$

Figure 2 illustrates the upper limits for the all-blazar

neutrino flux from *Fermi* 2LAC and *Fermi* 3LAC analysis. In the left panel, we assume $s = 2$ for the neutrino spectrum. In this case, the stacking analysis of *Fermi*-2LAC blazars gives $1.2 \times 10^{-8} \lesssim E_\nu^2 \Phi_{E_\nu}^{(2LAC, \text{stacking})} \lesssim 1.6 \times 10^{-8}$ (in the unit of $\text{GeV cm}^{-2} \text{ s}^{-1} \text{ sr}^{-1}$, hereafter). The corresponding upper limits for all blazars calculated using equation 7 are illustrated as the magenta area. The green area in the left panel shows the constraints derived from *Fermi*-3LAC analysis which predicts $8.0 \times 10^{-9} \lesssim E_\nu^2 \Phi_{E_\nu}^{(3LAC, \text{stacking})} \lesssim 1.4 \times 10^{-8}$. For illustration purposes, we include the IceCube all-flavor neutrino flux $4.8 \times 10^{-8} \lesssim E_\nu^2 \Phi_{E_\nu}^{(IC)} \lesssim 8.4 \times 10^{-8}$ in Figure 2 (the cyan area). The right panel shows the energy-dependent upper limits for an $\varepsilon_\nu^{-2.5}$ neutrino spectrum. The solid lines are obtained by assuming $\gamma_{lw} = 1.0$ whereas the dashed lines correspond to the case $\gamma_{lw} = 2.0$. The upper limits from *Fermi* 2LAC and 3LAC analysis are illustrated as magenta lines and blue lines, respectively. In this figure, we showed also the 3-flavor averaged neutrinos flux (red points; Aartsen et al. 2015a, 2016), the 6-year high-energy starting events (cyan points; Aartsen et al. 2017c) and the best fit to the upcoming muon neutrinos scaled to three-flavor (yellow area). The previous discussion reveals that $\mathcal{F}(\gamma_{lw})$ depends sensitively on $L_{ph,min}$ when γ_{lw} is smaller than 1.0. We will demonstrate in §3 that, in the range $\gamma_{lw} \lesssim 1.0$, the neutrino multiplet constraints are more stringent than the upper limits derived from the stacking analyses.

3. IMPLICATIONS OF HIGH-ENERGY NEUTRINO MULTIPLET LIMITS

Assuming the number of sources that produce more than $k - 1$ multiplet events is $N_{m \geq k}$, the constraint from the non-detection of $m \geq k$ multiplet events can be obtained by requiring $N_{m \geq k} \leq 1$. Murase & Waxman (2016) studied the implications to the neutrino sources using the absence of “high-energy” multiplet neutrino sources, and calculated the upper limit on the local source number density for an ε_ν^{-2} neutrino spectrum,

$$n_0^{\text{eff}} \lesssim 1.9 \times 10^{-10} \text{ Mpc}^{-3} \left(\frac{\varepsilon_\nu L_{\varepsilon_\nu}^{\text{ave}}}{10^{44} \text{ erg s}^{-1}} \right)^{-3/2} \left(\frac{b_m q_L}{6.6} \right)^{-1} \times \left(\frac{F_{\text{lim}}}{10^{-9.2} \text{ GeV cm}^{-2} \text{ s}^{-1}} \right)^{3/2} \left(\frac{2\pi}{\Delta\Omega} \right), \quad (8)$$

where $\varepsilon_\nu L_{\varepsilon_\nu}^{\text{ave}}$ is the time-averaged neutrino luminosity of the source, $F_{\text{lim}} \sim (5 - 6) \times 10^{-10} \text{ GeV cm}^{-2} \text{ s}^{-1}$ is the 8-year IceCube point-source sensitivity at the 90% confidence level (Aartsen et al. 2017b), $q_L \sim 1 - 3$ denotes a luminosity-dependent correction factor, $\Delta\Omega$ represents the sky coverage of the detector and the details of $m \geq k$ multiplet analysis are encoded in the factor b_m . Murase & Waxman (2016) find $b_m \simeq 6.6$ for $m \geq 2$ multiplets and $b_m \simeq 1.6$ for triplets or higher multiplets (e.g. $m \geq 3$).

The purpose of this work reveals the implications for blazar models not making new analyses on multiplets. We simply use the results of the previous analysis by Murase & Waxman (2016), which gives the upper limit

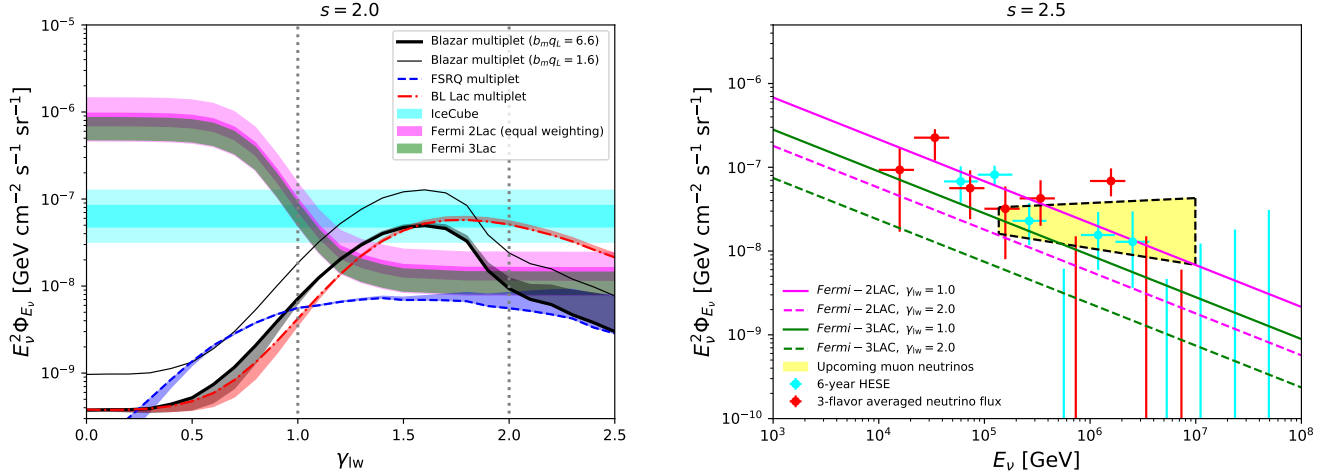


FIG. 2.— Left panel: Stacking constraints on the contribution of all blazars to the cumulative neutrino flux and high-energy multiplet constraints on the blazar contribution in the neutrino sky for an ε_ν^{-2} neutrino spectrum. The magenta and green areas correspond to the all-blazar upper limit from *Fermi*-2LAC equal weighting and *Fermi*-3LAC analysis, respectively. The cyan horizontal area shows the cumulative neutrino flux detected by IceCube. The blue dashed, red dash-dotted and thick black lines illustrate the $m \geq 2$ multiplet constraints for FSRQs, BL Lacs and all blazars whereas the corresponding areas show the uncertainties. The thin black line is the $m \geq 3$ multiplet constraint for all blazars. Right panel: the energy-dependent upper limits for the neutrino flux from all blazars, assuming a neutrino spectral index $s = 2.5$.

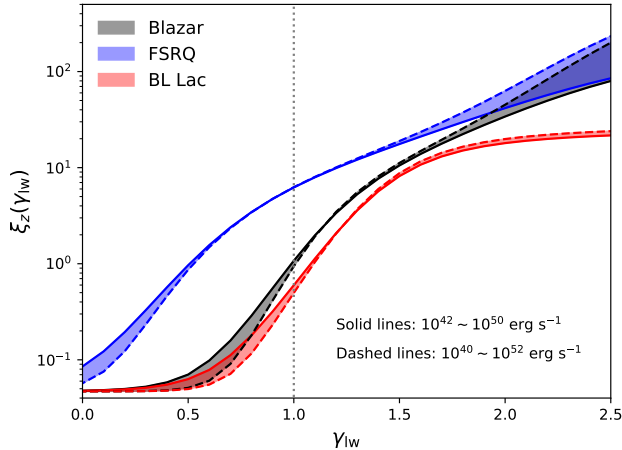


FIG. 3.— The redshift evolution factor ξ_z for FSRQs (blue area), BL Lacs (red area) and all blazars (black area). The solid and dashed boundaries correspond to different schemes of $L_{\text{ph,min}}$ and $L_{\text{ph,max}}$.

on the effective number density, $n_0^{\text{eff}}(\varepsilon_\nu L_{\varepsilon_\nu}^{\text{ave}})$. These are also consistent with the latest limits on transient sources (after the number density is converted into the rate density, e.g. Aartsen et al. 2019). One can write the limit on the cumulative neutrino flux from the sources as a function of n_0^{eff} and the redshift evolution factor ξ_z (Murase et al. 2018):

$$\begin{aligned}
 E_\nu^2 \Phi_{E_\nu}^{(m)} &\approx \frac{3\xi_z c t_H}{4\pi} n_0^{\text{eff}}(\varepsilon_\nu L_{\varepsilon_\nu}^{\text{ave}}) \\
 &\lesssim 6.9 \times 10^{-9} \left(\frac{\Delta\Omega}{2\pi}\right)^{2/3} \left(\frac{\xi_z}{0.7}\right) \left(\frac{b_m q_L}{6.6}\right)^{-2/3} \\
 &\times \left(\frac{n_0^{\text{eff}}}{10^{-7} \text{ Mpc}^{-3}}\right)^{1/3} \left(\frac{F_{\text{lim}}}{10^{-9.2} \text{ GeV cm}^{-2} \text{ s}^{-1}}\right), \quad (9)
 \end{aligned}$$

where t_H is the Hubble time. In this expression, ξ_z represents the redshift weighting of the neutrino luminosity of the sources and can be evaluated through (Waxman & Bahcall 1998)

$$\xi_z(\gamma_{\text{lw}}) = \frac{\int dz (1+z)^{-1} \left| \frac{dt}{dz} \right| f(z, \gamma_{\text{lw}})}{\int dz \left| \frac{dt}{dz} \right|}, \quad (10)$$

where $f(z, \gamma_{\text{lw}})$ is the redshift evolution function of the neutrino luminosity density normalized to unity at $z = 0$ for the luminosity correlation $L_\nu \propto L_{\text{ph}}^{\gamma_{\text{lw}}}$, e.g. for blazars we have $f^{(\text{bl})}(z, \gamma_{\text{lw}}) = [\varepsilon_\nu Q_\nu^{(\text{bl,all})}(z, \gamma_{\text{lw}})] / [\varepsilon_\nu Q_\nu^{(\text{bl,all})}(0, \gamma_{\text{lw}})]$. Similarly, we can also calculate the ξ_z for the blazar subclasses, FSRQs and BL Lacs using the luminosity functions from Ajello et al. (2012, 2013). The black, blue and red areas in Figure 3 illustrate the redshift evolution factor $\xi_z(\gamma_{\text{lw}})$ for all blazars, FSRQs and BL Lacs, respectively. When $\gamma_{\text{lw}} = 1$, we find $\xi_z \sim 7 - 8$ for the gamma-ray luminosity density evolution of FSRQs and $\xi_z \sim 0.6 - 0.7$ for that of BL Lacs, which are consistent with the values found by Murase et al. (2014) and Murase & Waxman (2016). The solid and dashed boundaries in Figure 3 correspond to the sample schemes, ($L_{\text{ph,min}} = 10^{42} \text{ erg s}^{-1}$, $L_{\text{ph,max}} = 10^{50} \text{ erg s}^{-1}$) and ($L_{\text{ph,min}} = 10^{40} \text{ erg s}^{-1}$, $L_{\text{ph,max}} = 10^{52} \text{ erg s}^{-1}$), respectively. If γ_{lw} is lower than 1.0, low-luminosity sources at lower redshift contribute a significant component to the total neutrino luminosity density, therefore, a smaller $L_{\text{ph,min}}$ results in a smaller ξ_z . On the contrary, a strong luminosity correlation with $\gamma_{\text{lw}} \gtrsim 1.5$ boosts the contribution from high-redshift bright blazars, which leads to a larger $f(z, \gamma_{\text{lw}})$ at higher redshift and as a result makes ξ_z larger, as $L_{\text{ph,max}}$ increases.

Besides the factor ξ_z , and the effective local number density n_0^{eff} , which characterizes the the number density of sources that dominate the neutrino luminosity density, it is also necessary to calculate the neutrino

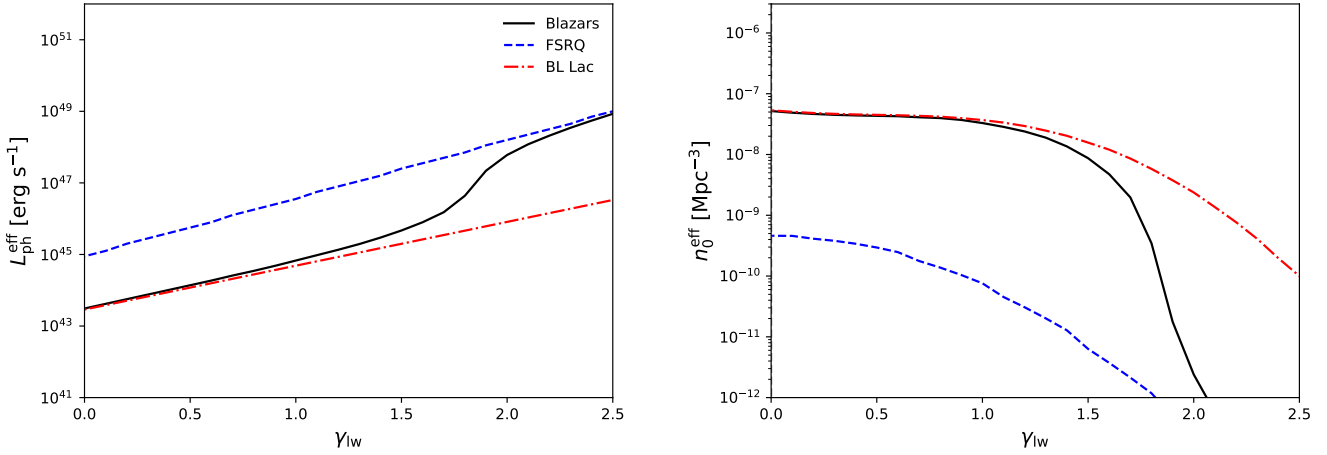


FIG. 4.— Left panel: The effective gamma-ray luminosity for FSRQs (blue dashed line), BL Lacs (red dash-dotted line) and all blazars (black line). Right panel: The effective local number densities for different source classes. The line styles in this panel have the same meaning as the left panel.

multiplet upper limits for one specified source population. In this work, we use the luminosity functions in combination with the luminosity weighting relation $L_\nu \propto L_{\text{ph}}^{\gamma_{\text{lw}}}$ to estimate the effective number densities n_0^{eff} for blazars, FSRQs and BL Lacs. Here, we follow the procedure presented by Murase & Waxman (2016). For each class of neutrino sources, we define an effective neutrino luminosity $L_\nu^{\text{eff}} \propto (L_{\text{ph}}^{\text{eff}})^{\gamma_{\text{lw}}}$ using the corresponding effective gamma-ray luminosity $L_{\text{ph}}^{\text{eff}}$ obtained by maximizing $L_{\text{ph}}^{\gamma_{\text{lw}}} (dN/d\ln L_{\text{ph}}) = L_{\text{ph}}^{\gamma_{\text{lw}}+1} \phi(L_{\text{ph}}, z=0)$, where $\phi(L_{\text{ph}}, z=0)$ is the local luminosity function of the sources that we are interested in. The left panel of Figure 4 shows the effective gamma-ray luminosity densities for all blazars (black solid line), FSRQs (blue dashed line) and BL Lacs (red dash-dotted line). Intuitively, $L_{\text{ph}}^{\text{eff}}$ of FSRQ should be larger than that of BL Lacs since FSRQs are more luminous than BL Lacs. Moreover, the function $L_{\text{ph}}^{\gamma_{\text{lw}}+1} \phi(L_{\text{ph}}, z=0)$ achieves its maximum at higher luminosity as γ_{lw} increases, which naturally explains the monotonic increase of $L_{\text{ph}}^{\text{eff}}(\gamma_{\text{lw}})$. Considering that low-luminosity BL Lacs dominate the neutrino luminosity density if the luminosity correlation is weak (e.g. $\gamma_{\text{lw}} \lesssim 1$) whereas bright FSRQs become increasingly important as γ_{lw} increases, the blazar effective luminosity $L_{\text{ph}}^{\text{eff}}$ converges to the BL Lac case when γ_{lw} is less than 1.0 and then gradually approaches to the FSRQ curve, as is confirmed in Figure 4. With the effective neutrino/gamma-ray luminosity, we can write down the effective local number density of the sources

$$n_0^{\text{eff}} = \frac{1}{L_{\text{ph}}^{\text{eff}}} \int dL_{\text{ph}} L_\nu(L_{\text{ph}}) \phi(L_{\text{ph}}, 0). \quad (11)$$

The right panel of Figure 4 shows the effective number densities of all blazars (black solid line), FSRQs (blue dashed line) and BL Lacs (red dash-dotted line). As expected, BL Lacs dominate the number density and the blazar effective number density converges to BL Lac and FSRQ curves respectively when $\gamma_{\text{lw}} \lesssim 1.0$ and $\gamma_{\text{lw}} \gtrsim 2.0$. Different from $\mathcal{F}(\gamma_{\text{lw}})$ and ξ_z , $L_{\text{ph}}^{\text{eff}}$ and n_0^{eff}

does not depend sensitively on the value of $L_{\text{ph},\text{min}}$ and $L_{\text{ph},\text{max}}$ in the range $0 \lesssim \gamma_{\text{lw}} \lesssim 2.5$. To interpret this, we need to keep in mind that the former two quantities are determined by the integrations over L_{ph} , while $L_{\text{ph}}^{\text{eff}}$ depends only on the shape/slope of the function $L_{\text{ph}}^{\gamma_{\text{lw}}+1} \phi(L_{\text{ph}}, z=0)$. From the left panel of Figure 4, we find that $L_{\text{ph}}^{\text{eff}}$ lies roughly in the range $10^{43} - 10^{49} \text{ erg s}^{-1}$ which is covered by the interval $10^{42} - 10^{50} \text{ erg s}^{-1}$ used in our calculation. Meanwhile, the integrand in equation 11 peaks around $L_{\text{ph}}^{\text{eff}}$, therefore once the peak is included, the effective number density n_0^{eff} will not vary too much as the lower and upper bounds of the integral changes.

The above calculations provide the preliminary work and the ingredients needed for calculating the neutrino multiplet limits. Selecting $b_m q_L \simeq 6.6$ for $m \geq 2$ multiplets and $F_{\text{lim}} \simeq 10^{9.2} \text{ GeV cm}^{-2} \text{ s}^{-1}$ for an ε_ν^{-2} neutrino spectrum, the blue dashed, red dashed-dotted and thick black lines in the left panel of Figure 2 illustrate the multiplet limits for FSRQs, BL Lacs and all blazars, respectively. The blue, red and black areas shows the corresponding uncertainties due to $L_{\text{ph},\text{min}}$ and $L_{\text{ph},\text{max}}$, as discussed before. From this figure we find that the all-blazar multiplet constraint converges to the FSRQ case at higher γ_{lw} and to the BL Lac case if γ_{lw} is less than 1.0 just as expected. We also considered the upper limits for triplet or higher multiplets ($m \geq 3$) by changing the value of $b_m q_L$ to 1.6. In this case, the constraints relax to the thin black line. This consequence can be interpreted as the concession of allowing blazars to produce $m = 2$ multiplet events. So far, all calculations on the multiplet constraints were based on the ε_ν^{-2} neutrino spectrum, and to extend the results to a general spectrum, e.g., $s = 2.5$, detailed calculations on F_{lim} and n_0^{eff} (equation 11) are needed, and our results are conservative in this point.

4. DISCUSSION

In this paper, we considered two types of constraints on the contribution of blazars to the cumulative neutrino flux assuming a luminosity weighting $L_\nu \propto L_{\text{ph}}^{\gamma_{\text{lw}}}$. Using the gamma-ray luminosity functions for blazars, FS-

RQs and BL Lacs, we estimated the ratio of the neutrino fluxes from resolved blazars and from all blazars, $\mathcal{F}(\gamma_{lw})$, and the effective number densities, $n_0^{\text{eff}}(\gamma_{lw})$, and the redshift evolution factor, ξ_z , for different source classes. The main results are summarized in Figure 2. From this figure we found that the multiplet constraints are the most important at lower values of γ_{lw} , e.g. $\gamma_{lw} \lesssim 1.0$, whereas all-blazar constraints derived from stacking constraints on resolved blazars are stronger for a strong luminosity correlation. Canonical blazar models, which are physically motivated and based on the leptonic scenario, predict $\gamma_{lw} \sim 1.5 - 2.0$ (Murase et al. 2014). Our results suggest that the stacking constraints are the most stringent for such physically motivated cases. The multiplet and stacking limits are complementary, as pointed out by Murase et al. (2018). In the range where the stacking limits are weak (for $\gamma_{lw} \lesssim 1.3$), the multiplet limits become more stringent. We also found that while the multiplet constraints are weaker at larger values of γ_{lw} they become more stringent again for $\gamma_{lw} \gtrsim 1.5$ due to the rapid decrease of the effective source density.

In this work, we focus on power-law spectra. The limits are stringent for the neutrino flux in the 0.1 PeV range and become weaker at higher energies. For example, multiplet limits are weaker if one is interested in the origin of ~ 1 PeV neutrinos (Murase & Waxman 2016; Murase et al. 2018; Palladino et al. 2019). It is possible for blazars to explain the dominant fraction of PeV neu-

trinos by introducing a lower-energy cutoff of the proton maximum energy (Dermer et al. 2014), although neutrinos at 0.1 PeV and lower energies should come from another population of the sources.

One of the uncertainties in this work come primarily from the selection of the lower and upper limits of the luminosity integral, $L_{\text{ph,min}}$ and $L_{\text{ph,max}}$. As discussed above, we showed that these uncertainties are well controlled, and the final results are reliable if $L_{\text{ph,min}}$ and $L_{\text{ph,max}}$ are selected in the fiducial ranges $10^{40} - 10^{42} \text{ erg s}^{-1}$ and $10^{50} - 10^{52} \text{ erg s}^{-1}$, respectively. From the joint constraints illustrated in Figure 2, we conclude that blazars are disfavored as a dominant source of the cumulative cumulative neutrino flux measured by IceCube for a luminosity weighting $L_\nu \propto L_{\text{ph}}^{\gamma_{lw}}$ with $0.0 \lesssim \gamma_{lw} \lesssim 2.5$. Since different blazar models considered for explaining the cumulative neutrino flux can be commonly characterized by the correlation index γ_{lw} within this range, our calculations on the upper limits and effective number densities would provide rather general constraints for future studies of blazar neutrinos.

We thank Marco Ajello for useful discussion on the usage of the luminosity function. The work of K.M. is supported by the Alfred P. Sloan Foundation and NSF grant No. PHY-1620777, while that of C.C.Y. and P.M. is supported by the Eberly Foundation.

REFERENCES

- Aartsen, M., Abbasi, R., Abdou, Y., et al. 2013a, *Physical review letters*, 111, 021103
—, 2013b, *Science*, 342, 1242856
Aartsen, M., Ackermann, M., Adams, J., et al. 2014a, *Physical review letters*, 113, 101101
—, 2014b, *The Astrophysical Journal*, 796, 109
Aartsen, M., Abraham, K., Ackermann, M., et al. 2015a, *The Astrophysical Journal*, 809, 98
Aartsen, M., Ackermann, M., Adams, J., et al. 2015b, *The Astrophysical Journal*, 807, 46
—, 2015c, *Physical review letters*, 114, 171102
Aartsen, M., Abraham, K., Ackermann, M., et al. 2016, *The Astrophysical Journal*, 833, 3
—, 2017a, *The Astrophysical Journal*, 835, 45
Aartsen, M., Ackermann, M., Adams, J., et al. 2017b, *arXiv preprint arXiv:1710.01179*
Aartsen, M. G., et al. 2017c, *arXiv: 1710.01191*
Aartsen, M. G., Ackermann, M., Adams, J., et al. 2019, *Phys. Rev. Lett.*, 122, 051102
Abdo, A., Ackermann, M., Ajello, M., et al. 2010, *The Astrophysical Journal*, 720, 435
Ahlens, M., & Halzen, F. 2014, *Physical Review D*, 90, 043005
—, 2015, *Reports on Progress in Physics*, 78, 126901
Ahlens, M., & Murase, K. 2014, *Physical Review D*, 90, 023010
Ajello, M., Shaw, M., Romani, R., et al. 2012, *The Astrophysical Journal*, 751, 108
Ajello, M., Romani, R., Gasparrini, D., et al. 2013, *The Astrophysical Journal*, 780, 73
Ajello, M., Gasparrini, D., Sánchez-Conde, M., et al. 2015, *The Astrophysical Journal Letters*, 800, L27
Ando, S., Feyereisen, M. R., & Fornasa, M. 2017, *Phys. Rev. D*, 95, 103003.
<https://link.aps.org/doi/10.1103/PhysRevD.95.103003>
Dekker, A., & Ando, S. 2019, *Journal of Cosmology and Astro-Particle Physics*, 2019, 002
Dermer, C. D., Murase, K., & Inoue, Y. 2014, *Journal of High Energy Astrophysics*, 3, 29
Feyereisen, M. R., Tamborra, I., & Ando, S. 2017, *Journal of Cosmology and Astro-Particle Physics*, 2017, 057
Glauch, T., Turcati, A., & IceCube Collaboration. 2017, *International Cosmic Ray Conference*, 301, 1014
Hooper, D., Linden, T., & Vieregge, A. 2018, *arXiv preprint arXiv:1810.02823*
IceCube Collaboration, et al. 2018, *Science*, 361, eaat1378
IceCube Collaboration, Aartsen, M. G., Ackermann, M., et al. 2019, *The European Physical Journal C*, 79, 234.
<https://doi.org/10.1140/epjc/s10052-019-6680-0>
Mészáros, P. 2017, *Annual Review of Nuclear and Particle Science*, 67, 45
Murase, K. 2017, in *neutrino astronomy: current status, future prospects* (World Scientific), 15–31
Murase, K., Inoue, Y., & Dermer, C. D. 2014, *Physical Review D*, 90, 023007
Murase, K., Oikonomou, F., & Petropoulou, M. 2018, *The Astrophysical Journal*, 865, 124
Murase, K., & Waxman, E. 2016, *Physical Review D*, 94, 103006
Neronov, A., & Semikoz, D. 2018, *arXiv preprint arXiv:1811.06356*
Neronov, A., Semikoz, D. V., & Ptitsyna, K. 2017, *Astronomy & Astrophysics*, 603, A135
Padovani, P., Petropoulou, M., Giommi, P., & Resconi, E. 2015, *Mon. Not. Roy. Astron. Soc.*, 452, 1877
Palladino, A., Rodrigues, X., Gao, S., & Winter, W. 2019, *The Astrophysical Journal*, 871, 41
Petropoulou, M., Dimitrakoudis, S., Padovani, P., Mastichiadis, A., & Resconi, E. 2015, *Monthly Notices of the Royal Astronomical Society*, 448, 2412
Pinat, E., & Sánchez, J. A. A. 2017, *PoS*, 963
Righi, C., Tavecchio, F., & Guetta, D. 2017, *A&A*, 598, A36
Rodrigues, X., Fedynitch, A., Gao, S., Boncioli, D., & Winter, W. 2018, *ApJ*, 854, 54
Tavecchio, F., & Ghisellini, G. 2015, *Monthly Notices of the Royal Astronomical Society*, 451, 1502
Waxman, E., & Bahcall, J. 1998, *Physical Review D*, 59, 023002